Supplementary Information: Revealing the bonding of solvated Ru complexes with valence-to-core resonant inelastic x-ray scattering

Elisa Biasin*[1], Daniel R. Nascimento[2], Benjamin I. Poulter[3], Baxter Abraham[4], Kristjan Kunnus[1,5], Angel T. Garcia-Esparza[4], Stanislaw H. Nowak[4], Thomas Kroll[4], Robert W. Schoenlein[1,5], Roberto Alonso-Mori[5], Munira Khalil[3], Niranjan Govind*[2], and Dimosthenis Sokaras*[4]

[1]Stanford PULSE Institute, SLAC National Accelerator Laboratory, Menlo Park, CA 94025, USA.
[2]Physical and Computational Sciences Directorate, Pacific Northwest National Laboratory, Richland, Washington 99352, USA.
[3]Department of Chemistry, University of Washington, Seattle, Washington 98195, USA
[4]SSRL, SLAC National Accelerator Laboratory, Menlo Park, California 94025, USA
[5]LCLS, SLAC National Accelerator Laboratory, Menlo Park, CA 94025, USA.

Contents

1 Acquisition time

$[Ru^{II}(bpy)_3]^{2+}$: non-resonant VtC-XES (1h 50m); 2p4d RIXS spectrum measured at the PFY-XAS B peak (20m)
$[Ru^{II}(CN)_6]^{4-}$: non-resonant VtC-XES (1h 30m); 2p4d RIXS spectrum measured at the PFY-XAS B peak (26m); 2p4d RIXS spectrum measured at the PFY-XAS C peak (1h 46m)
$[Ru^{II}(bpy)_2Cl_2]$:non-resonant VtC-XES (40m); 2p4d RIXS spectrum measured at the PFY-XAS B peak (50 m)
$[Ru^{III}(NH_3)_6]^{3+}$: non-resonant VtC-XES (2h); 2p4d RIXS spectrum measured at the PFY-XAS A peak (26m); Bpeak (50m)
$[Ru^{III}(NH_3)_5Cl]^{2+}$: non-resonant VtC-XES (40m); A peak (1h 20m); 2p4d RIXS spectrum measured at the PFY-XAS B peak (26m)

2 Effective charge and ligand field strength effects on XAS and XES peak positions

Supplementary Figure 1a,b show the correlation between the energy of the 2p orbitals and the main spectral feature in the Ru L-edge XAS or non-resonant XES spectra, respectively, for the Ru-complexes investigated in this study. The energy of the 2p orbitals decreases (i.e. 2p orbitals are closer to the core) with increasing oxidation state due to the reduced screening. The position of the XAS and XES spectral feature report on the oxidation state, but also on ligand field strength. With respect to the XAS, the B position of the $[Ru^{II}(CN)_6]^{4-}$spectra is at higher energy because of the high ligand field splitting energy. More details are given in the main text. With respect to the VtC XES spectra, Supplementary Fig. 1b shows that the peak **a** position correlates with the energy of the 2p orbitals (which are lowest in energy for $[Ru^{III}(NH_3)_6]^{3+}$ and highest in energy for the $[Ru^{II}(CN)_6]^{4-}$). Therefore, the oxidation state information is encoded in the peak **a** energy shift: peak **a** is at lower energy for the Ru(II)-complexes with respect to the Ru(III)-complexes. Moreover, for complexes with the same oxidation state, both experiments and calculations (see also Table 2 in the text) show a shift of peak **a** to the higher energy side for complexes with stronger ligand field, according to the spectrochemical series.

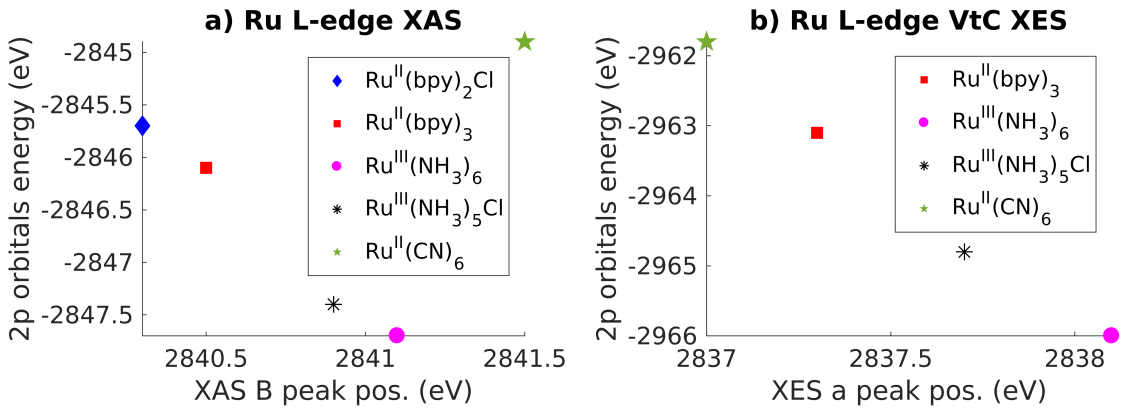

Supplementary Figure 1. a) Correlation between the energies of the 2p orbitals in the ground-state and the position of the B peak in the XAS PFY spectra shown in Figure 1 of the main article. b) Correlation between the energies of the 2p orbitals in the core-hole ionized system and the position of the **a** peak in the VtC XES spectra shown in Figure 2 of the main article.

Supplementary Table 1. Orbital energies (eV) of the ground and core-hole ionized state of the Ru model complexes, relevant for understanding the observed trends in the L_3-XAS and VtC-XES spectra.

Ground state					
	$[Ru^{II}(bpy)_2Cl_2]$	$[Ru^{II}(bpy)_3]^{2+}$	$[Ru^{III}(NH_3)_6]^{3+}$	$[Ru^{III}(NH_3)_5Cl]^{2+}$	$[Ru^{II}(CN)_6]^{4-}$
2p	-2845.7	-2846.1	-2847.7	-2847.4	-2844.9
4d(π)		-6.0655	-6.1215	-5.7693	-4.8552
4d(σ)		-2.0564	-1.2181	-1.1405	2.2657
Core-hole ionized state					
	$[Ru^{II}(bpy)_2Cl_2]$	$[Ru^{II}(bpy)_3]^{2+}$	$[Ru^{III}(NH_3)_6]^{3+}$	$[Ru^{III}(NH_3)_5Cl]^{2+}$	$[Ru^{II}(CN)_6]^{4-}$
2p	-2962.6	-2963.1	-2966.0	-2964.8	-2961.8
4d(π)		-9.06	-10.72	-9.508	-7.2565

3 Ground state orbitals labelling

The molecular orbitals (MOs) are a linear combination of (non-orthogonal) atomic base functions. After optimization, we print all the contributions to each of the MOs and we identify the MOs that contain Ru 4d character and group them according to their energy. For each MO, the linear coefficients are normalized so that the sum of the squared coefficients is 1. For each group of MOs of the same (or similar) energy (for instance, for the three 4d(π) orbitals), we calculate the percent contribution of each atomic base function to the total. Only the principal angular momentum is considered (for instance an N p orbital comprises N pz, N px, and N py). The results of this analysis are summarized in Table 1 in the main article, while the pictures of the MOs for each Ru-complex can be find in Supplementary Tables 2-4.

$[Ru^{III}(NH_3)_5Cl]^{2+}$			
4d(σ)	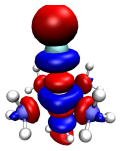		
4d(π)	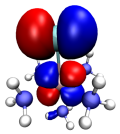	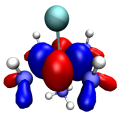	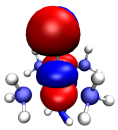
Cl(π)		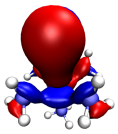	
NH3(σ)		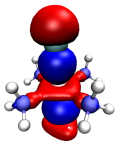	
$[Ru^{III}(NH_3)_6]^{3+}$			
4d(σ)	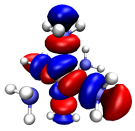	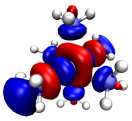	
4d(π)	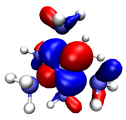	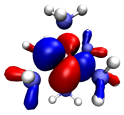	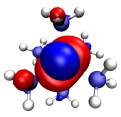
NH3(σ)	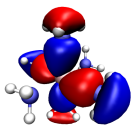	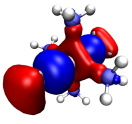	

Supplementary Table 2. GS orbitals of the Ru(III)-complexes

$[Ru^{II}(CN)_6]^{4-}$			
CN(π^*)	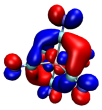	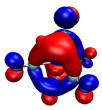	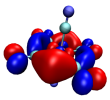
4d(σ)			
4d(π)	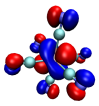	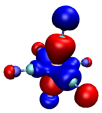	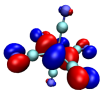
CN(5σ)	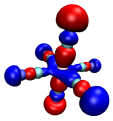		
CN(π)	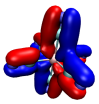	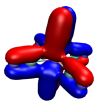	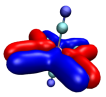
CN(4σ)	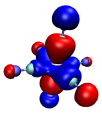		

Supplementary Table 3. GS orbitals of the $[Ru^{II}(CN)_6]^{4-}$ complex

	$[Ru^{II}(bpy)_3]^{2+}$		
4d(σ)		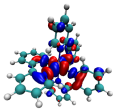	
bpy(π^*)	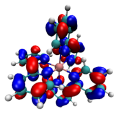	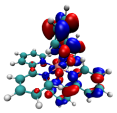	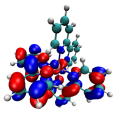
4d(π)		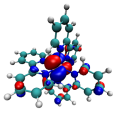	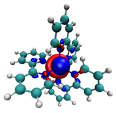
bpy(σ)	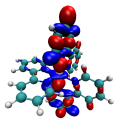	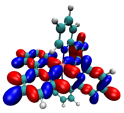	

Supplementary Table 4. GS orbitals of the $[Ru^{II}(bpy)_3]^{2+}$ complex

4 Analysis of non-resonant 4d → 2p XES data and calculations

4.1 Peak fitting of the spectra

The TDDFT calculated 4d → 2p non-resonant spectra are fitted with a sum of Lorentzian functions. Panel b, d, f, h of Supplementary Fig. 2 show the results for, respectively, the calculated spectra of $[Ru^{II}(CN)_6]^{4-}$, $[Ru^{II}(bpy)_3]^{2+}$, $[Ru^{III}(NH_3)_6]^{3+}$, and $[Ru^{III}(NH_3)_5Cl]^{2+}$. For the last two complexes, the main peak (peak **a** in the main text) is fitted with two Lorentzian functions and the position of the maximum of the sum of the two peaks is reported in Table 2 of the main article.

The measured non-resonant 4d → 2p spectra are fitted with a sum of Voigt profiles. The peak positions, intensities, Lorentzian and Gaussian FWHM are free parameters, but the Gaussian FWHM is constrained between 0.3 and 0.4 eV, while the Lorentzian FWHM is constrained between 1 and 2 eV.

For $[Ru^{II}(CN)_6]^{4-}$(Supplementary Fig. 2a) and $[Ru^{II}(bpy)_3]^{2+}$(Supplementary Fig. 2c) a Voigt peak centered at high energy side with respect to the main peak is used to fit the high energy side shoulder in the data. This is most likely due to multi-electron excitations, and therefore not reproduced by the TDDFT calculations. For $[Ru^{II}(bpy)_3]^{2+}$, $[Ru^{III}(NH_3)_6]^{3+}$(Supplementary Fig. 2e), and $[Ru^{III}(NH_3)_5Cl]^{2+}$(Supplementary Fig. 2g) only one Voigt profile is used to fit the low energy side feature. Finally, for $[Ru^{III}(NH_3)_6]^{3+}$, the main peak is described by two Voigt profile. The two function are summed and the position of the maximum of the sum is reported in Table 2 of the main text.

Supplementary Table 5 report the peak positions of the experimental data determined by the fit and the 95 % confidence intervals.

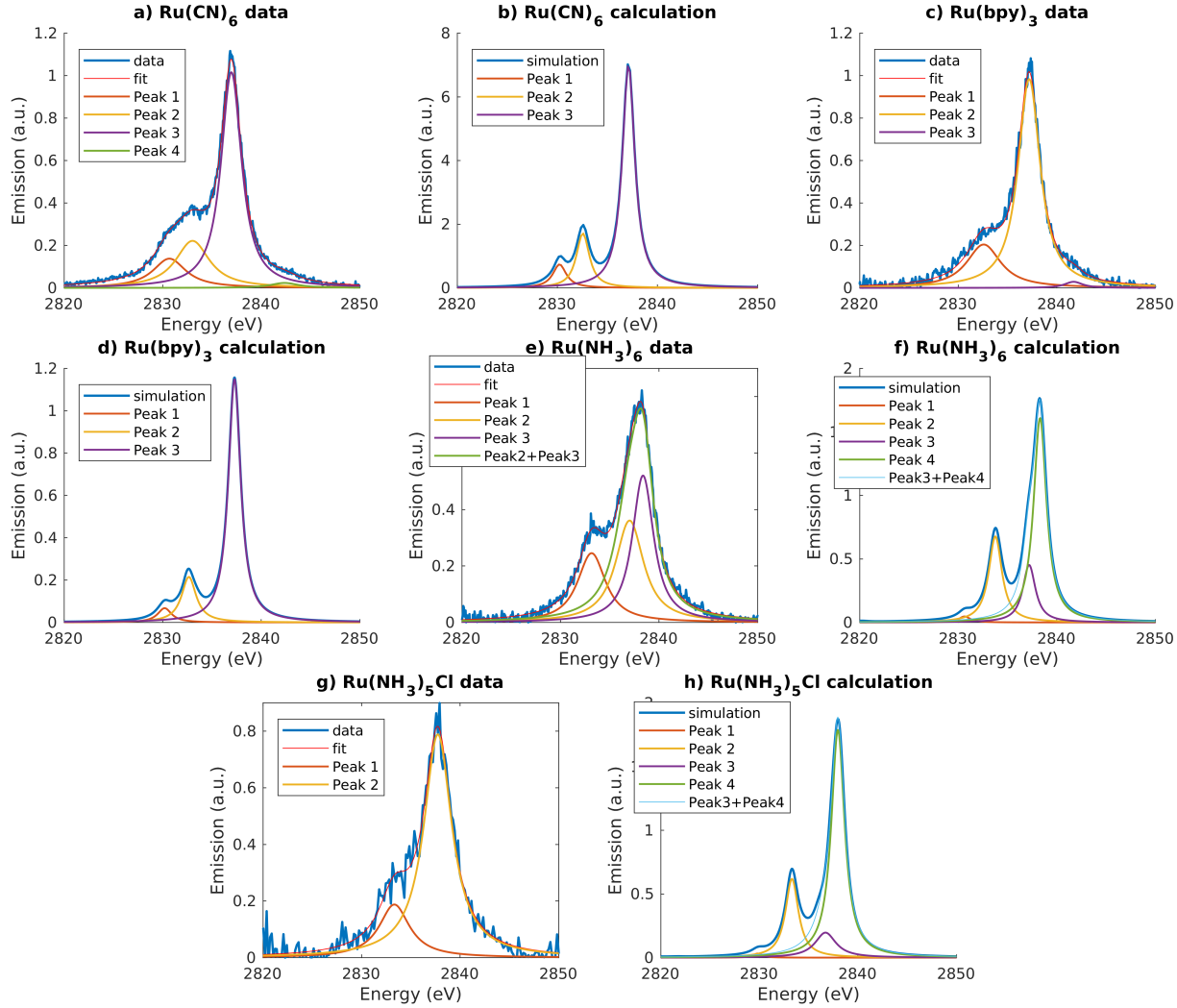

Supplementary Figure 2. Results of fitting a sum of Voigt functions and a sum of Lorentzian functions to the experimental and calculated spectra, respectively.

4.2 Character of non-resonant 4d → 2p spectral features

For the spectral decomposition in terms of atomic orbitals (results reported in Table 2), we followed procedure used in Ref. [3]. Each calculated discrete transition (root r) is described as a combination of single-electron transitions t from a valence molecular orbital (VOs) to the 2p-hole. For each root, we calculate the contribution of the atomic orbitals of type o as:

$$c_o^r = O_r \sum_{VO} S_{VO} \sum_i c_{o,i}^{VO} \tag{1}$$

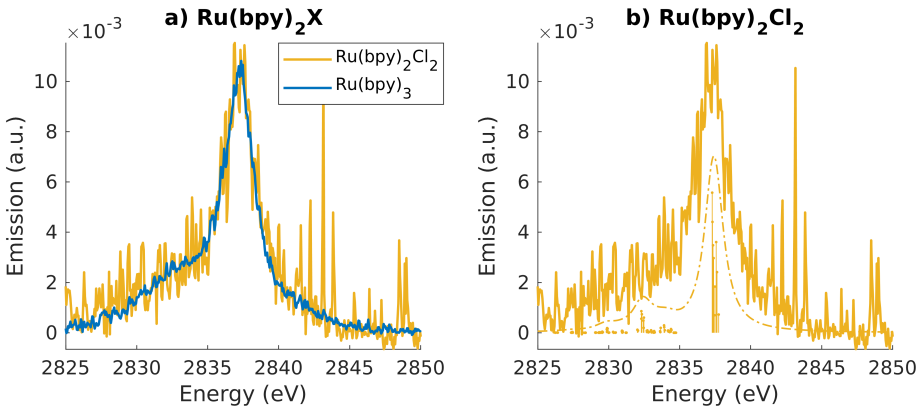

Supplementary Figure 3. a) Comparison between $[Ru^{II}(bpy)_2Cl_2]$ and $[Ru^{II}(bpy)_3]^{2+}$ 4d $\rightarrow$ 2p non-resonant emission spectra. Low signal to noise for the $[Ru^{II}(bpy)_3]^{2+}$ spectrum arises from low concentration (10 mM) of the sample and low acquisition time. b) Measured (solid line) and calculated (dashed line) of 4d $\rightarrow$ 2p non-resonant emission spectra of $[Ru^{II}(bpy)_2Cl_2]$.

Supplementary Table 5. Peak position in non-resonant 4d $\rightarrow$ 2p emission spectra. Reported errors for the experimental data are 95 % confidence intervals. For the calculated spectra, the errors are smaller than 0.1 eV.

Molecule	**Peak**	**Pos. (eV)**	
		Exp.	Calc.
$[Ru^{III}(NH_3)_5Cl]^{2+}$	a	2737.7 ± 0.1	2838.0
	b	2833.3 ± 0.3	2833.3
	c	n.a.	2829.8
$[Ru^{III}(NH_3)_6]^{3+}$	a	2838.1 ± 0.1	2838.2
	b	2833.2 ± 0.2	2833.8
	c	n.a.	2830.6
$[Ru^{II}(CN)_6]^{4-}$	a	2837.0 ± 0.1	2837.1
	b	2833.0 ± 0.3	2832.5
	c	2830.7 ± 0.4	2830.2
$[Ru^{II}(bpy)_3]^{2+}$	a	2837.3 ± 0.1	2837.3*
	b	n.a.	2832.7
	c	n.a.	2830.2

* A global shift of 96.3 eV is applied to the calculated spectra
n.a. = peak is not well-defined in the experimental data

where O_r is the oscillator strength of root r, S_{VO} describes the contribution of valence molecular orbital to transition r, normalized such that $\sum_{VO} S^2_{VO}$ =1, index i runs over the number of atomic orbitals of type o (for instance orbital of type Np is further decomposed in Npx, Npy, and Npz). For each molecular orbital, $\sum_o \sum_i c^{VO}_{o,i}$ =1. In our analysis, only the 10 most dominant atomic orbitals contributions to each VO are considered.

Finally, the percentage contribution c of the atomic orbitals of type o to a collection of roots within a specific energy range is given by:

$$c_o = \frac{\sum_r c_o^r}{\sum_r \sum_o c_o^r} \tag{2}$$

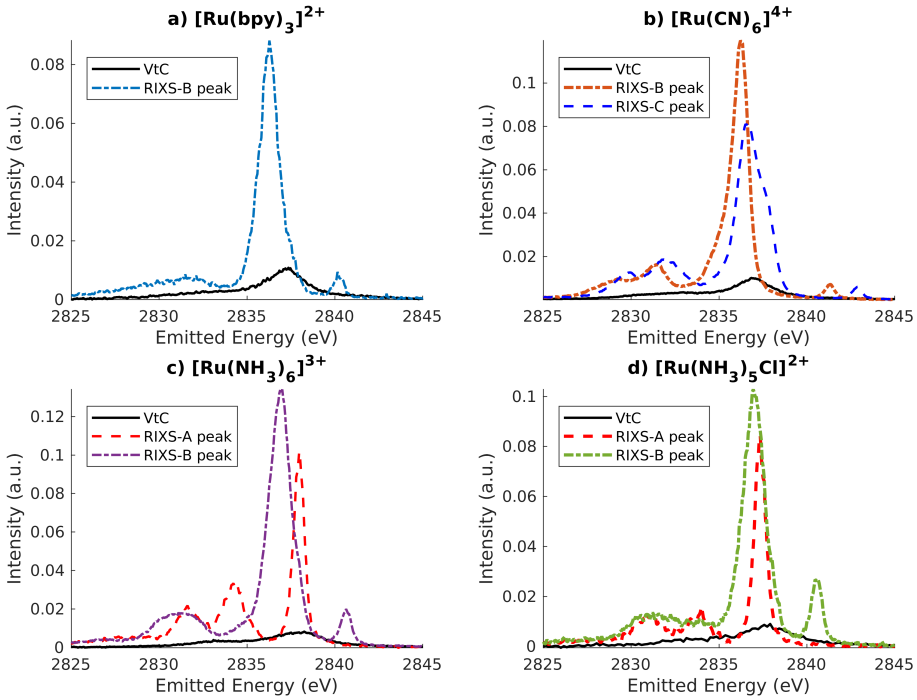

Supplementary Figure 4. Non-resonant and resonant 4d → 2p emission as a function of emitted energy for the Ru-model complexes investigated in this work. For each complex, all the spectra are normalized to the area of the non-resonant VtC-XES spectrum and therefore the relative intensities can be directly compared.

5 4d-4d multiplet effects

In this work, we consider the energy of the MC states measured by the 2p4d RIXS equivalent to the ligand field splitting energies. This is based on the fact that 4d-4d multiplet effects can be neglected. In octahedral symmetry, and on a first approximation, the MC state energy (with respect to the ground state) can be calculated as $\Delta E(1T_{1g}$ - $1A_{1g}) = 10Dq$ - C, where 10Dq is the ligand field splitting energy and C is the Racah parameter. We calculate the C Racah parameter from the Slater integrals describing the direct electron-electron interactions (C=35F_4) and considering a scaling of 25% with respect to the atomic Hartree-Fock value [1]. For both a Ru(II) and Ru(III) atom, we find C = 0.1 eV. This value is consistent with the dd multiplet effects reported for Fe-complexes, and considering that, for 4d systems: 1) the Slater integrals are reduced more than the corresponding 3d systems; and 2) the atomic values themselves are also smaller [1]. For instance, dd multiplet effects are reported to

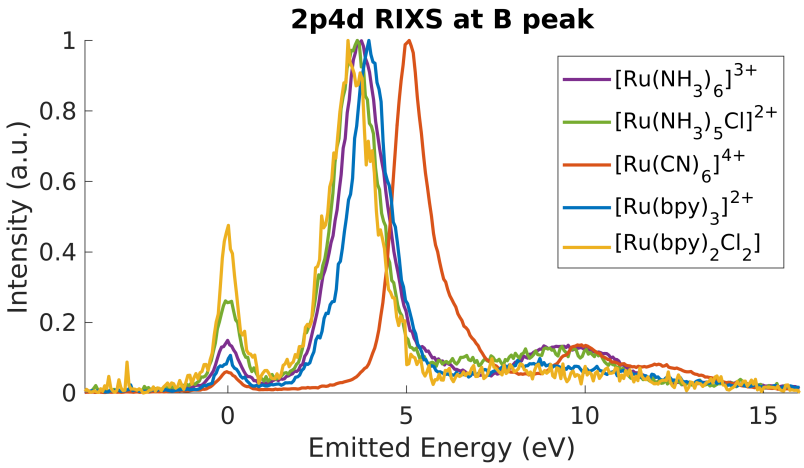

Supplementary Figure 5. 4d2p RIXS measured resonantly at the B peak of the PFY-XAS spectra for the Ru-model complexes investigated in this work. The spectra are shown as a function of energy transfer and they have been normalized to the main peak, which reports on the energy of the MC state for each complex.

be on the order of 0.3 eV for $[Fe^{II}(CN)_6]^{4-}$ [2] and also for mixed tetracyano-polypyridyl Fe-complexes [4]. We note that dd multiplet effects for 4d systems have been considerably less investigated than for 3d materials.

6 Molecular Structures

6.1 $[Ru^{II}(bpy)_3]^{2+}$

Ru 0.000000 0.000000 0.000000
N 1.824945 0.031723 1.049294
N 1.410074 -0.161141 -1.554830
C 2.944700 -0.051523 0.282167
C 1.958719 0.151307 2.380715
C 3.191283 0.192897 3.009561
C 4.340183 0.108675 2.234032
C 4.212279 -0.012277 0.859299
C 2.712955 -0.183268 -1.166187
C 1.121758 -0.270072 -2.862430
C 2.096178 -0.404617 -3.836499
C 3.429295 -0.429802 -3.448631
C 3.736594 -0.319798 -2.101568
H 1.042458 0.211759 2.949461
H 3.239263 0.288636 4.085352
H 5.320782 0.139577 2.689821
H 5.095652 -0.075143 0.241450
H 0.074290 -0.245172 -3.124872
H 1.806116 -0.487001 -4.874731
H 4.218437 -0.536556 -4.180852
H 4.768286 -0.342011 -1.783529
N -0.224137 -2.092048 -0.060645
N -1.721393 -0.228596 -1.190129
C -1.275754 -2.549226 -0.791540
C 0.590486 -2.982118 0.530237
C 0.406026 -4.350304 0.428217
C -0.664954 -4.826222 -0.316648
C -1.509765 -3.915635 -0.931565
C -2.123173 -1.510515 -1.401359
C -2.444755 0.772748 -1.718239
C -3.585645 0.556890 -2.472053
C -4.003146 -0.748943 -2.693137
C -3.264715 -1.788610 -2.150281
H 1.410923 -2.573530 1.101707
H 1.092450 -5.020645 0.926519
H -0.839834 -5.888721 -0.420681
H -2.345419 -4.269689 -1.516637
H -2.087415 1.773726 -1.526003
H -4.128212 1.401262 -2.873943
H -4.890563 -0.956599 -3.275959
H -3.577689 -2.809671 -2.309916

N -1.253763 0.346009 1.655182
N -0.033797 2.102664 0.100752
C -1.474845 1.652297 1.961740
C -1.856565 -0.603328 2.390102
C -2.695763 -0.310016 3.451319
C -2.927523 1.021245 3.771409
C -2.312130 2.007874 3.017147
C -0.775565 2.630199 1.111139
C 0.629045 2.934898 -0.719534
C 0.589757 4.311869 -0.582245
C -0.164779 4.859337 0.446990
C -0.849941 4.008635 1.300079
H -1.650964 -1.626299 2.111119
H -3.152821 -1.115260 4.009432
H -3.579117 1.289221 4.592335
H -2.485655 3.047773 3.250512
H 1.204025 2.471844 -1.508062

6.2 $[\mathbf{Ru^{II}(bpy)_2Cl_2}]$

Ru 0.00000000 0.00000000 0.00000000
Cl 2.22035045 -0.04849079 1.07525781
Cl 0.97508021 -0.13061045 -2.26205861
N -0.20792268 -2.06860075 -0.07532165
N -1.85074136 -0.20495608 -0.89333514
C -1.30942772 -2.52497654 -0.72694378
C 0.69619226 -2.95296603 0.37894108
C 0.54091938 -4.31900892 0.21771667
C -0.58753472 -4.79927222 -0.43961957
C -1.51768968 -3.89112560 -0.91766404
C -2.23739535 -1.47993259 -1.17482136
C -2.66038347 0.80665571 -1.25305472
C -3.86922929 0.61007096 -1.89417539
C -4.27335201 -0.68934679 -2.18559780
C -3.44738730 -1.73807174 -1.81887167
H 1.55747648 -2.51224343 0.86497634
H 1.29658889 -4.99109470 0.60196420
H -0.73739614 -5.86161869 -0.58291075
H -2.39795701 -4.24196368 -1.43699959
H -2.30584743 1.79970639 -1.01860422
H -4.47782731 1.46398708 -2.15958045
H -5.21273990 -0.88037205 -2.68760817
H -3.74041272 -2.75593281 -2.03217193
N -0.78951839 0.35196958 1.87612172

N 0.09402740 2.07431991 0.11742998
C -0.77219516 1.64758693 2.29508333
C -1.26155909 -0.58845991 2.71331193
C -1.73331170 -0.29834956 3.97991064
C -1.72024709 1.02280168 4.41702012
C -1.23618167 1.99878688 3.56281408
C -0.26497965 2.61248719 1.31236358
C 0.56350325 2.88176630 -0.84877250
C 0.68477340 4.24979961 -0.67581048
C 0.31194677 4.81413117 0.54016010
C -0.16407186 3.98469663 1.54210941
H -1.24377155 -1.60222692 2.34079778
H -2.10094097 -1.09786415 4.60893851
H -2.08019187 1.28627164 5.40291902
H -1.21697142 3.03159068 3.87959927
H 0.85135967 2.37665073 -1.76217414
H 1.06757061 4.85810520 -1.48439963
H 0.39624438 5.88019029 0.70739514
H -0.45268657 4.40150337 2.49627110

6.3 $[\mathbf{Ru^{III}(NH_3)_6}]^{3+}$

Ru 0.000000 0.000000 0.000000
N -0.004325 -0.010462 2.163711
N 0.022569 2.160275 -0.002920
N -2.158348 -0.028645 -0.044423
N -0.022281 -2.160244 0.002488
N 0.004277 0.010032 -2.163663
N 2.158347 0.029037 0.044826
H -0.938569 -0.056713 2.573050
H 0.490612 -0.807871 2.564960
H -2.586117 0.724948 0.496925
H -2.550494 0.077382 -0.980766
H -0.894794 -2.566047 -0.337601
H 0.701131 -2.575459 -0.587544
H -0.484599 0.811018 -2.565212
H 0.938883 0.049178 -2.572903
H 2.572443 0.882875 -0.330548
H 2.550310 -0.074187 0.981546
H -0.703031 2.575743 0.584198
H 0.893873 2.566103 0.340215
H -0.437089 -0.807854 -2.585405
H -0.122465 2.576935 -0.922843
H -2.572601 -0.883437 0.328618

H 0.126173 -2.577147 0.921727
H 2.586433 -0.726009 -0.494210
H 0.430997 0.810542 2.585697

6.4 $[\mathbf{Ru^{III}(NH_3)_5Cl}]^{2+}$

Ru 0.00000000 0.00000000 0.00000000
N 0.00297754 0.08041971 2.18686046
N 0.07668638 2.15866666 -0.12546046
N -2.16249624 -0.01073447 -0.03353356
N -0.07084032 -2.16220111 0.03786778
Cl -0.00169038 -0.09105604 -2.31615160
N 2.16285810 0.00711800 -0.04596637
H -0.60099716 0.82102616 2.54226273
H -0.32777900 -0.77363466 2.63335637
H -2.61582260 0.81412253 0.35649504
H -2.45191234 -0.05311712 -1.01141117
H -0.90896523 -2.56831979 0.44997773
H -0.05249539 -2.48120188 -0.93143672
H 2.60699893 0.84722606 0.32057452
H 2.61836497 -0.77206265 0.42702491
H -0.72953010 2.65577033 0.25047399
H 0.88950962 2.59279163 0.30815462
H 0.11752489 2.40346011 -1.11552271
H -2.60303999 -0.80526717 0.42664664
H 0.71172975 -2.62241323 0.50062413
H 2.44476314 -0.05455604 -1.02496795
H 0.91956841 0.26708060 2.59099274

6.5 $[\mathbf{Ru^{II}(CN)_6}]^{4-}$

Ru 0.000000 0.000000 0.000000
C -1.999157 0.074465 -0.558178
N -3.127380 0.115747 -0.875238
C -0.067319 2.009341 0.523221
N -0.103331 3.143972 0.816958
C -0.557376 -0.528044 1.929663
N -0.872294 -0.823528 3.019985
C 0.066417 -2.009027 -0.524763
N 0.096497 -3.143590 -0.819500
C 0.560349 0.527890 -1.928805
N 0.879132 0.827407 -3.016927
C 1.998971 -0.076462 0.558153

N 3.126858 -0.114606 0.876855

References

[1] F. M. F. de Groot, Z. W. Hu, M. F. Lopez, G. Kaindl, F. Guillot, and M. Tronc. Differences between l3 and l2 x[U+2010]ray absorption spectra of transition metal compounds. *The Journal of Chemical Physics*, 101(8):6570–6576, 1994.

[2] H. B. Gray and N. A. Beach. The electronic structures of octahedral metal complexes. i. metal hexacarbonyls and hexacyanides. *Journal of the American Chemical Society*, 85(19):2922–2927, Oct 1963.

[3] W. M. Holden, E. P. Jahrman, N. Govind, and G. T. Seidler. Probing sulfur chemical and electronic structure with experimental observation and quantitative theoretical prediction of kα and valence-to-core kβ x-ray emission spectroscopy. *The Journal of Physical Chemistry A*, 124(26):5415–5434, 2020.

[4] K. Kunnus, L. Li, C. J. Titus, S. J. Lee, M. E. Reinhard, S. Koroidov, K. S. Kjær, K. Hong, K. Ledbetter, W. B. Doriese, G. C. O'Neil, D. S. Swetz, J. N. Ullom, D. Li, K. Irwin, D. Nordlund, A. A. Cordones, and K. J. Gaffney. Chemical control of competing electron transfer pathways in iron tetracyano-polypyridyl photosensitizers. *Chem. Sci.*, 11:4360–4373, 2020.